npj | Quantum Materials

www.nature.com/npjquantmats

ARTICLE OPEN

Check for updates

Pressure-induced topological superconductivity in the spin–orbit Mott insulator $GaTa_4Se_8$

Moon Jip Park[1,2], GiBaik Sim[1,2], Min Yong Jeong[1,2], Archana Mishra[1], Myung Joon Han[1]✉ and SungBin Lee[1]✉

Lacunar spinel $GaTa_4Se_8$ is a unique example of spin–orbit coupled Mott insulator described by molecular $j_{eff} = 3/2$ states. It becomes superconducting at $T_c = 5.8$ K under pressure without doping. In this work, we show, this pressure-induced superconductivity is a realization of a new type topological phase characterized by spin-2 Cooper pairs. Starting from first-principles density functional calculations and random phase approximation, we construct the microscopic model and perform the detailed analysis. Applying pressure is found to trigger the virtual interband tunneling processes assisted by strong Hund coupling, thereby stabilizing a particular *d*-wave quintet channel. Furthermore, we show that its Bogoliubov quasiparticles and their surface states exhibit novel topological nature. To verify our theory, we propose unique experimental signatures that can be measured by Josephson junction transport and scanning tunneling microscope. Our findings open up new directions searching for exotic superconductivity in spin–orbit coupled materials.

npj Quantum Materials (2020)5:41 ; https://doi.org/10.1038/s41535-020-0246-0

INTRODUCTION

The confluence of spin–orbit coupling (SOC) and strong electron correlation provides a new paradigm of solid-state quantum phenomena[1–6]. In particular, the new type of superconductivity that are expected to arise in spin–orbit coupled Mott insulators has drawn great attentions. The representative candidate materials are transition metal dicalchogenides TaS_2[6] and Sr_2IrO_4[1,2,7–11]. Despite of the promising examples, the microscopic superconducting mechanism itself, as well as its pairing symmetry remain, elusive. The key step forward is to have a concrete material platform for which the unambiguous theoretical description can be provided and tested. In addition, reliable prediction of pairing symmetry and the detailed suggestions for its experimental verification are demanded.

Lacunar spinel compounds, GaM_4X_8 (M = transition metals; X = chalcogens), are a fascinating class of materials for the demonstration of rich correlated electronic structure and potential applications in technologies[12–21]. Among the known lacunar spinels, $GaTa_4Se_8$ is a Mott insulator with a charge gap of 0.1–0.3 eV[22–24]. Its widely tunable conductivity is expected to be useful for nonvolatile memory devices[24–27]. More recent first-principles calculation points out that the SOC of Ta ion induces a novel electronic band structure described by molecular state with so-called $j_{eff} = 3/2$ nature[28]. Subsequently, resonant inelastic X-ray scattering (RIXS) experiment has directly verified this $j_{eff} = 3/2$ electronic structure[29], establishing $GaTa_4Se_8$ as a notable example of spin–orbit coupled Mott insulator where both electron correlation and SOC play the crucial role.

Strikingly, applying pressure induces the phase transition from a spin–orbit coupled Mott insulator to a metal and eventually to a superconductor[22,30–32]. The characteristics of this superconductivity are quite intriguing in many regards. First, $GaTa_4Se_8$ does not show any long-range magnetic order down to low temperature[22,30]. Second, there is no experimental signature for structural transition as a function of pressure and no drastic phonon mode change. Third, nevertheless, the anomalies in specific heat as well as magnetic susceptibility are repeatedly identified at around 50 K, which is an order of magnitude higher than superconducting T_c[22,33–36]. Most importantly, it is also noted that superconductivity is only observed in the case of M = Nb and Ta; namely, only when the low energy band structure is of $j_{eff} = 3/2$ character[28]. This observation heavily prompts a speculation that $j_{eff} = 3/2$ nature of the electronic band structure pervades the origin of the superconductivity, being different from the conventional BCS type. However, there has been no firm investigation on its character both theoretically and experimentally.

In this paper, we show that the superconductivity in $GaTa_4Se_8$ is attributed to the new type of electronic pairing. Due to the intriguing interplay of multi-band $j_{eff} = 3/2$ character and inter-band correlation, novel *d*-wave quintet superconductivity with spin-2 Cooper pairs is stabilized. Such high angular momentum Cooper pair state has been also referred to as the quintet pairing states[37–43]. Utilizing both density functional theory and random phase approximation (RPA), we first show that the system well retains the characteristic of $j_{eff} = 3/2$ under high pressure. Our first-principles calculations also show how intra-, inter-orbital electron interactions and Hund coupling change by pressure. Starting from the constructed many-body Hamiltonian, we analytically show that applying pressure activates many-body inter-band tunnelings and opens attractive quintet pairing channels assisted by strong Hund coupling. Among the possible quintet pairings, it turns out the system favors a particular *d*-wave superconductivity with t_{2g} symmetries. This novel superconductivity is characterized by nodal lines of Bogoliubov quasiparticles and by topologically protected Majorana modes at the surface. Thereby, our work theoretically establishes $GaTa_4Se_8$ as a strong candidate of topological *d*-wave superconductor. In order to facilitate its confirmation, we also propose the concrete experimental setups and the signatures to be identified in Josephson junction transport and scanning tunneling microscopy (STM).

[1]Department of Physics, KAIST, Daejeon 34141, Republic of Korea. [2]These authors contributed equally: Moon Jip Park, GiBaik Sim, Min Yong Jeong. ✉email: mj.han@kaist.ac.kr; sungbin@kaist.ac.kr

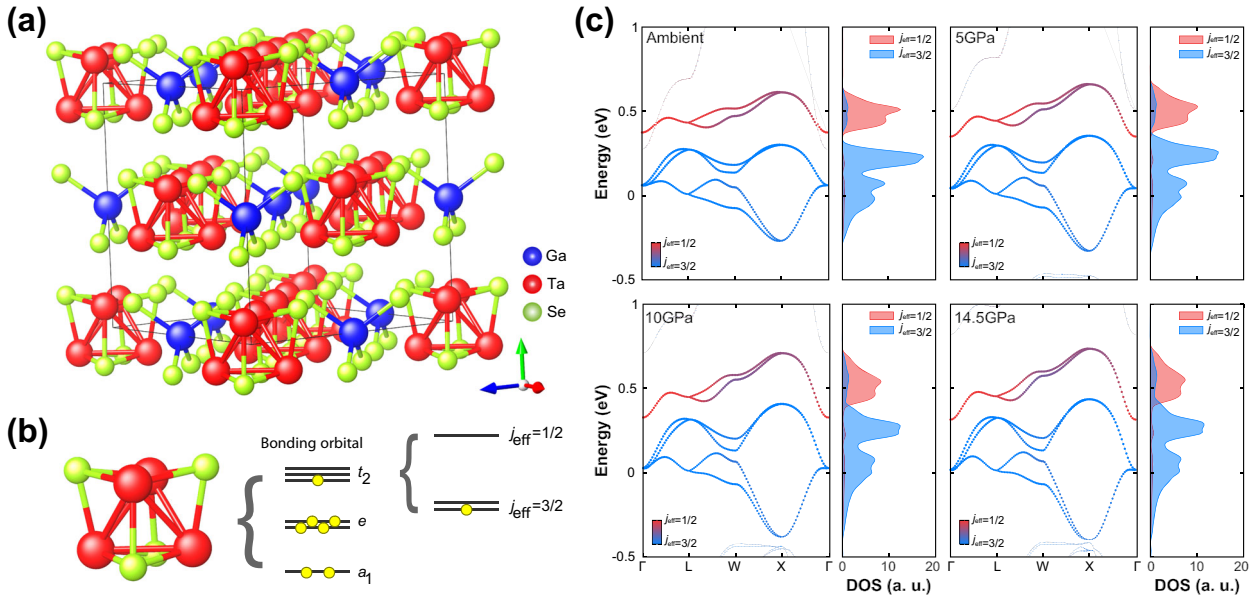

Fig. 1 Crystal and band structure of $GaTa_4Se_8$. a Crystal structure of $GaTa_4Se_8$. $GaSe_4$, and Ta_4Se_4 clusters consist of NaCl-like structure. **b** Schematic electronic structure near Fermi level. Molecular bonding orbitals e and a_1 are fully-filled and one electron is in t_2 orbitals. By SOC, t_2 orbitals split into $j_{eff} = 1/2$ doublet and $j_{eff} = 3/2$ quartet with one electron in $j_{eff} = 3/2$ bands. **c** Fat bands and PDOS of $GaTa_4Se_8$ for various pressures (ambient, 5 GPa, 10 GPa, and 14.5 GPa). Even under high pressure, $j_{eff} = 3/2$ bands are well separated from other bands.

RESULTS

Electronic structure and many-body Hamiltonian

$GaTa_4Se_8$ consists of $GaSe_4$ and Ta_4Se_4 clusters arranged in NaCl structure (see Fig. 1a)[22] that belong to the space group $F\bar{4}3m$, which forms non-centrosymmetric structure. Due to the short intra-cluster bondings, its electronic band structure is well understood by molecular orbital states, and the states near Fermi level are dominated by triply degenerate molecular t_2 orbitals denoted by (D_{xy}, D_{yz}, D_{zx})[22]. Just as the atomic t_{2g} orbitals, molecular t_2 can also be represented by effective angular momentum $l_{eff} = 1 = -L_{(1)}$ where $L_{(1)}$ is the angular momentum operator with orbital quantum number $l = 1$[44]. The spin–orbit interaction, $H_{SOC} = -\lambda \boldsymbol{l} \cdot \boldsymbol{S}$, gives rise to the molecular quartet $j_{eff} = 3/2$ and the doublet $j_{eff} = 1/2$. In particular, molecular quartet $j_{eff} = 3/2$ in the basis of $|j, j^z>$ is being represented as $|3/2, \pm 3/2> = \mp\frac{1}{\sqrt{2}}(|D_{yz,\uparrow\downarrow}\rangle \pm i|D_{zx,\uparrow\downarrow}\rangle)$ and $|3/2, \pm 1/2> = \sqrt{\frac{2}{3}}(|D_{xy,\uparrow\downarrow}\rangle \mp \frac{|D_{yz,\downarrow\uparrow}\rangle \pm i|D_{zx,\downarrow\uparrow}\rangle}{2})$ where $\uparrow, \downarrow$ refer to spin directions[28].

The calculated band dispersions and the projected density of states (PDOS) are shown in Fig. 1c as a function of pressure (for more details, see Supplementary Information 1 and ref. [22] for the crystal structure data under the pressures). Note that, not only at the ambient pressure but at the high pressure up to 14.5 GPa, $j_{eff} = 3/2$ band characters are well maintained and still dominating the near Fermi energy region. It justifies our low energy model containing $j_{eff} = 3/2$ states.

In order to take into account electronic correlations, we construct many-body Hamiltonian including intra-orbital ($U > 0$), inter-orbital interaction ($U' > 0$) and Hund coupling ($J_H > 0$):

$$H_I = U\sum_u n_{u\uparrow}n_{u\downarrow} + U'\sum_{u,v<u} n_{u\sigma}n_{v\sigma'} + \frac{J_H}{2}\sum_{u\neq v,\sigma,\sigma'} d^\dagger_{u\sigma}d^\dagger_{v\sigma'}d_{u\sigma'}d_{v\sigma} + \frac{J_H}{2}\sum_{u\neq v,\sigma\neq\sigma'} d^\dagger_{u\sigma}d^\dagger_{u\sigma'}d_{v\sigma'}d_{v\sigma} \quad (1)$$

where $d_{iu\sigma}$ ($d^\dagger_{iu\sigma}$) is the annihilation (creation) operator of electrons with orbital $u \in (D_{xy}, D_{yz}, D_{zx})$ and spin σ. The third and fourth terms are the Hund exchange and Hund's pair hopping interaction, respectively.

d-wave quintet pairing

Projecting this many-body interactions onto $j_{eff} = 3/2$ basis (namely, $\Psi = (|3/2\rangle, |1/2\rangle, |-1/2\rangle, |-3/2\rangle)$) and using Fierz transformation, Eq. (1) is exactly decoupled into the singlet and the five distinct quintet pairing channels as follow:

$$H_{I,J_{eff}=3/2} = g_0(\Psi^\dagger T^\dagger \Psi^*)(\Psi^T T\Psi) + g_1\sum_{a=1}^{3}(\Psi^\dagger(T\gamma_a)^\dagger\Psi^*)(\Psi^T T\gamma_a\Psi) + g_2\sum_{a=4}^{5}(\Psi^\dagger(T\gamma_a)^\dagger\Psi^*)(\Psi^T T\gamma_a\Psi). \quad (2)$$

Here, γ_a is the four-dimensional gamma matrices representing quintet-spin operator and T is the unitary component of the time-reversal operator (for more details, see Supplementary Information 3). g_1 and g_2 represent the quintet pairing strength with t_{2g} and e_g symmetry, respectively, while g_0 is the singlet pairing strength. Assuming that $j_{eff} = 3/2$ states are well separated from 1/2 bands, one can have the exact expression of each coupling constant: $g_0 = (2U + U' + 3J_H)/24$, $g_1 = (3U' - J_H)/24$ and $g_2 = (U + 2U' - 3J_H)/24$[45].

It is remarkable that no matter how large is the intra-orbital interaction U, g_1 coupling can be attractive and therefore induce superconducting instability if the Hund coupling is comparable to inter-orbital interaction, $J_H > 3U'$. In contrast, the singlet pairing channel cannot be attractive ($g_0 < 0$) since the Hund's coupling and the Hubbard interactions are both positive. This result is irrespective of the interaction parameters, which single out the possibility of the trivial singlet superconductivity.

Importantly, this t_{2g} symmetry d-wave pairing is robust even when the inter-band mixings between $j_{eff} = 3/2$ and 1/2 are considered. Figure 1c shows the band separation between $j_{eff} = 3/2$ and 1/2 gradually decreases as the pressure increases the bandwidth. At high enough pressure, the sizable many-body interband tunneling is expected. In this regime, $j_{eff} = 1/2$ can make

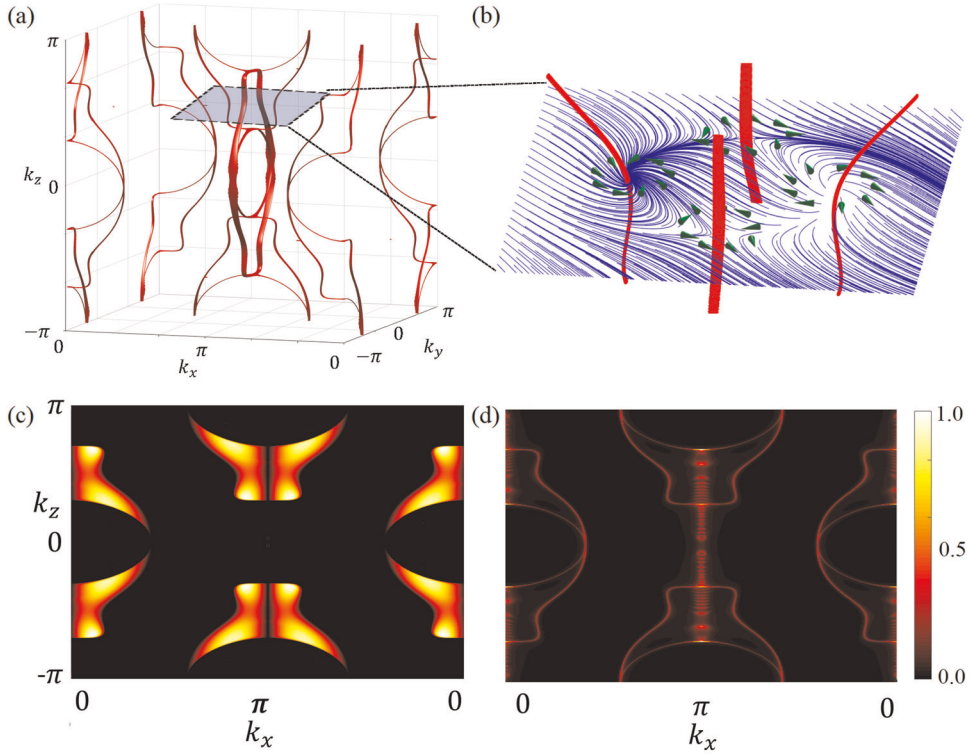

Fig. 2 Gap structure and topological surface states. a The BdG gap structure of d_{xy} pairing. We find two-fold degenerate nodal line gap structure shown as the red line. The red columns indicate the nodal lines. **b** The non-trivial winding of phase $\Phi(\mathbf{k})$ around the nodal lines. The blue streamline represents the winding of the phase $\Phi(\mathbf{k})$. We find that the non-trivial winding number protects the nodal line. **c**–**d** The normalized zero-energy spectral density of the surface (**c**) and bulk (**d**). Open surface possesses the topological Majorana flat band covering the interior of the nodal line. The open boundary condition is taken along [010]-direction.

an additional contribution to the effective pairing interaction, g, through the virtual tunneling process. This effect can formally be calculated using many-body Schrieffer–Wolff transformation[46]. Interestingly, we find, the leading order contribution of the interband tunneling is always attractive pairing interactions irrespective of the specific values of (U, U', J_H) (See Supplementary Information 3B for the estimation of the interaction parameters derived using the RPA calculation.) As a result, the tunneling effect, assisted by strong J_H, opens up the attractive superconducting channel characterized by $g_1 < 0$, and results in quintet-spin Cooper pairs with $t_{2g}d$-wave symmetry.

Topological superconductivity

The intriguing nature of this d-wave quintet Cooper pair can be found in its non-trivial spin texture originating from the unique topological property of Bogliubov-de Gennes (BdG) energy spectrum. Among the possible superconducting order parameter configurations with t_{2g} symmetry, we find that the energetically most favorable state, $\langle \psi^T T \vec{\gamma} \psi \rangle = (1,0,0)$-state where $\vec{\gamma} = (\gamma_1, \gamma_2, \gamma_3)$ represents quintet pairing with t_{2g} symmetry, is characterized by gapless nodal lines as shown in Fig. 2a; see Supplementary Information 4 for more details of our calculation. Due to the $j_{\text{eff}} = 3/2$ orbital character, the nodal lines in Fig. 2a exhibit robust d_{xy} symmetry even in the presence of small inversion symmetry breaking terms. This nodal lines have a topological origin and are protected by the non-trivial winding number.

It is first noted that the particle-hole and the time-reversal symmetry allow us to define the following non-hermitian matrix and its singular value decomposition, $h_0(\mathbf{k}) + iT|\Delta|\gamma_1 \equiv U_{\mathbf{k}}^{\dagger} D_{\mathbf{k}} V_{\mathbf{k}}$, where $h_0(\mathbf{k})$ is the normal Hamiltonian. $D_{\mathbf{k}}$ is now a diagonal matrix containing all the positive energy eigenvalues. Second, we can consider the adiabatic band flattening process by smoothly deforming $D_{\mathbf{k}}$ to $\mathbb{I}_4$ without any gap closing. This procedure defines the new unitary matrix, $q_{\mathbf{k}} \equiv U_{\mathbf{k}}^{\dagger} V_{\mathbf{k}} = \sum_n e^{i\lambda_n(\mathbf{k})} |n(\mathbf{k})\rangle\langle n(\mathbf{k})|$, and the corresponding phase $\lambda_n(\mathbf{k})$. These phases are well-defined as long as the system is fully gapped. Therefore, one can assign $\mathbb{Z}_2$ topological winding number along a line that encircles the nodal line as follow: $w = \frac{i}{2\pi} \oint d\mathbf{k} \cdot tr(q_{\mathbf{k}}^{\dagger} \nabla_{\mathbf{k}} q_{\mathbf{k}})$ according to DIII class in the Altland-Zirnbauer classifications[47].

Figure 2b shows the configuration of the phase $\Phi(\mathbf{k}) \equiv \sum_n \lambda_n(\mathbf{k})$. Blue streamlines clearly show that the phases have vortex–antivortex configurations where the core of the vortex defines the nodal line. From the explicit calculation of the winding number, we conclude that each nodal line and the vortex configuration are topologically characterized by the non-trivial winding number, $w = \pm 1$. These vortical configurations cannot be removed unless the vortex–antivortex pair annihilates each other. Thus, the nodal lines are topologically protected.

Experimental verifications

We now suggest the experimental signatures to verify d-wave quintet pairing. First of all, the non-trivial winding number encircling the nodal line manifests itself as the Majorana zero modes on the open surface. Figure 2c shows the simulated Majorana flat band, which can be directly observed by STM[48] and superconducting tunneling spectroscopy[49,50]. The Majorana zero-modes depicted in Fig. 2c exist in every momentum point in the interior of the surface projected nodal line. Thus the Majorana flat band contributes to the zero-energy density of state at the surface.

Another experiment we suggest is Josephson junction transport. Figure 3a–c show the current-phase relation (CPR) for the planar junction of rotating orientations. The CPR can be expressed

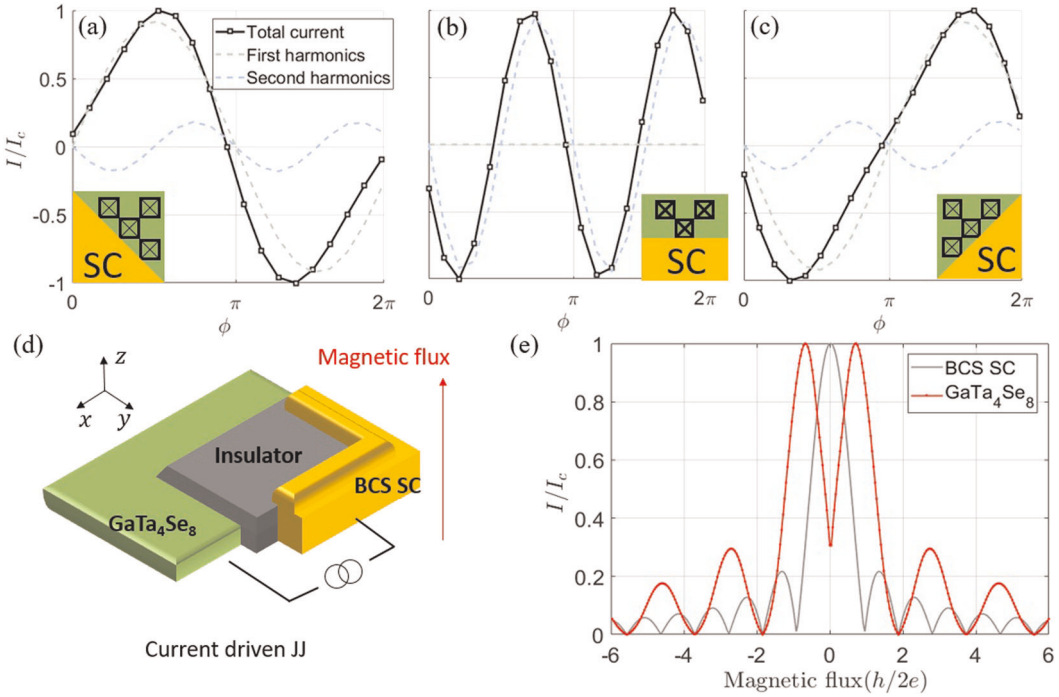

Fig. 3 Josephson junction experiment and Fraunhofer diffraction pattern. a–c The CPR of the planar Josephson junction at different orientations. Due to the d_{xy} pairing symmetry, the first harmonics of the CPR is inverted under 90° rotation. **d** Schematic figure of the Josephson corner junction. **e** The unconventional Fraunhofer pattern of the lacunar spinel. Unlike the conventional Fraunhofer pattern, the location of the peaks and the dips are reversed.

as a series of sinusoidal harmonics of the phase difference, ϕ: $I_J(\phi) = \sum_n I_n \sin(n\phi)$ where I_n gives the $2\pi n$ periodic Josephson current component. Due to the d_{xy} pairing symmetry, Josephson coupling gains π phase under 90° rotation of the junction orientation, and therefore the sign of I_1 is inverted as shown in Fig. 3a, c. In between the two angles (i.e., when the junction is formed along the [100]-direction), the first harmonics vanishes, $I_1 = 0$; see Fig. 3b. The next dominant CPR has π periodicity and the resulting Josephson frequency, $4eV/h$, is the twice of the conventional Josephson frequency[51]. This frequency doubling can be directly observed from the measurement of the Shapiro step in the I–V characteristics.

One can also make use of the pairing symmetry in this material which results in the unconventional magnetic oscillation pattern[52–56]. Figure 3d shows the schematic setup of the Josephson corner junction which is constructed on the corner of the lacunar spinel crystal. Due to the π-phase difference in CPR with different orientations, Josephson currents at each face destructively interfere with each other. However, because of small inversion symmetry breaking in the system, the critical current does not completely cancel but makes the dips in the Fraunhofer diffraction pattern as shown in Fig. 3e. As a consequence, we find that the overall locations of the peaks and the dips in the Fraunhofer pattern should be reversed compared to the case of conventional superconductors. This unusual magnetic oscillation pattern can be regarded as the signature of the quintet pairing in $GaTa_4Se_8$.

DISCUSSION

We discuss the relevance to another lacunar spinel material $GaNb_4Se_8$ which shares many similar features with $GaTa_4Se_8$. At ambient pressure, $GaNb_4Se_8$ is known to have a Mott gap of 0.19 eV[22], and the previous calculation shows that its low energy band character is also well-identified by $j_{\rm eff} = 3/2$ states due to the sizable SOC in Nb atoms[28]. The pressure-induced superconductivity is also found with $T_c = 2.9$ K at 13 GPa[30]. Such similarity with $GaTa_4Se_8$ may indicate $GaNb_4Se_8$ as another strong candidate of topological superconductors. Nevertheless, in contrast to $GaTa_4Se_8$, $GaNb_4Se_8$ has a sizable band overlap between $j_{\rm eff} = 3/2$ and $j_{\rm eff} = 1/2$ bands[28], which indicates the stronger interband tunneling effect that goes beyond the analysis of Schrieffer–Wolff transformation method. While stronger virtual tunneling effect on the superconductivity is expected, detailed correlation effect may be different under pressure, depending on molecular states occupied with either Nb or Ta.

In addition, Guiot et al. have performed Te doping in $GaTa_4Se_8$ by substitution of Se atoms[24]. The empirical effect of the Te doping is the reduction of the effective bandwidth followed by the increase of the Mott gap. Similarly, we may expect the increase of superconducting critical temperature. This would solidify our prediction that the superconducting pairing mediated by the electron-electron interaction than the phonon coupling.

Furthermore, the pressure control can be another interesting path to control the superconducting phase transition. Near the superconducting critical point, the transition to the time-reversal broken states is expected (See supplementary information 4). The time-reversal broken states is signatured by the Bogoliubov Fermi surfaces, and it can be measured by the anomalous thermal Hall effect similar to that of the $p + ip$ chiral superconductor. In general, the time-reversal broken phase cannot occur in conventional singlet pairing. Therefore, the thermal Hall effect near the superconducting phase transition would be another smoking gun signature of the quintet superconductivity.

In summary, we have suggested a new superconducting pairing mechanism for which spin–orbit entangled multiband nature plays an essential role together with electron correlation. Our theory is developed for and finds its relevance to $GaTa_4Se_8$ and other lacunar spinels, where the origin of pressure-induced superconductivity has not been understood for a long time. Starting from the realistic band structure and considering the correlation strengths calculated by first-principles DFT calculations, we have developed the detailed microscopic theory.

Superconducting gap is found to have *d*-wave symmetry and its gapless nodal lines emerge with the non-trivial topological character. Furthermore, we have proposed concrete experiments that can confirm our theoretical suggestion. The unusual *I–V* characteristics and the magnetic oscillation patterns are expected from Josephson transport and can be regarded as the smoking gun signatures for this quintet paring. STM image can also be compared with our results. Our findings will pave a new way to search for exotic superconductivity in lacunar spinel compounds.

METHODS

First-principles calculation

Electronic structures calculations were performed with OPENMX software package based on linear combination of pseudo-atomic-orbital basis[57] and within local density approximation (LDA)[58,59]. The SOC was treated within the fully relativistic j-dependent pseudo-potential scheme[60]. We used the $12 \times 12 \times 12$ k-grids for momentum-space integration and the experimental crystal structures at different pressures[22]. For the estimation of tight-binding hopping and interaction parameters, we used maximally localized Wannier function (MLWF) method[61,62] and constrained RPA (cRPA) technique[63–65] as implemented in ECALJ code[66].

DATA AVAILABILITY

The data that support the findings of this study are available from the corresponding author on reasonable request.

CODE AVAILABILITY

The computer code used for this study is available upon reasonable request.

Received: 25 January 2020; Accepted: 5 June 2020;
Published online: 24 June 2020

REFERENCES

1. Kim, B. J. et al. Phase-sensitive observation of a spin-orbital Mott state in Sr_2IrO_4. *Science* **323**, 1329–1332 (2009).
2. Kim, B. J. et al. Novel $J_{eff} = 1/2$ Mott state induced by relativistic spin-orbit coupling in Sr_2IrO_4. *Phys. Rev. Lett.* **101**, 076402 (2008).
3. Plumb, K. W. et al. $\alpha - RuCl_3$: a spin-orbit assisted Mott insulator on a honeycomb lattice. *Phys. Rev. B* **90**, 041112 (2014).
4. Orenstein, J. & Millis, A. J. Advances in the physics of high-temperature superconductivity. *Science* **288**, 468–474 (2000).
5. Sala, M. M. et al. $CaIrO_3$: a spin-orbit Mott insulator beyond the $j_{eff} = 1/2$ ground state. *Phys. Rev. Lett.* **112**, 176402 (2014).
6. Sipos, B. et al. From Mott state to superconductivity in 1T-TaS2. *Nat. Mater.* **7**, 960–965 (2008).
7. Yan, Y. J. et al. Electron-doped Sr_2IrO_4: an analogue of hole-doped cuprate superconductors demonstrated by scanning tunneling microscopy. *Phys. Rev. X* **5**, 041018 (2015).
8. Gao, Y., Zhou, T., Huang, H. & Wang, Q.-H. Possible superconductivity in Sr_2IrO_4 probed by quasiparticle interference. *Sci. Rep.* **5**, 9251 (2015).
9. Wang, F. & Senthil, T. Twisted Hubbard model for Sr_2IrO_4: magnetism and possible high temperature superconductivity. *Phys. Rev. Lett.* **106**, 136402 (2011).
10. Meng, Z. Y., Kim, Y. B. & Kee, H.-Y. Odd-parity triplet superconducting phase in multiorbital materials with a strong spin-orbit coupling: application to doped Sr_2IrO_4. *Phys. Rev. Lett.* **113**, 177003 (2014).
11. Watanabe, H., Shirakawa, T. & Yunoki, S. Monte Carlo study of an unconventional superconducting phase in iridium oxide $J_{eff} = 1/2$ Mott insulators induced by carrier doping. *Phys. Rev. Lett.* **110**, 027002 (2013).
12. Ruff, E. et al. Multiferroicity and skyrmions carrying electric polarization in GaV_4S_8. *Sci. Adv.* **1**, e1500916 (2015).
13. Reschke, S. et al. Optical conductivity in multiferroic GaV_4S_8 and GeV_4S_8 : Phonons and electronic transitions. *Phys. Rev. B* **96**, 144302 (2017).
14. Ruff, E. et al. Polar and magnetic order in GaV_4Se_8. *Phys. Rev. B* **96**, 165119 (2017).
15. Kézsmárki, I. et al. Néel-type skyrmion lattice with confined orientation in the polar magnetic semiconductor GaV_4S_8. *Nat. Mater.* **14**, 1116–1122 (2015).
16. Fujima, Y., Abe, N., Tokunaga, Y. & Arima, T. Thermodynamically stable skyrmion lattice at low temperatures in a bulk crystal of lacunar spinel GaV_4Se_8. *Phys. Rev. B* **95**, 180410 (2017).
17. Müller, H., Kockelmann, W. & Johrendt, D. The magnetic structure and electronic ground states of Mott insulators GeV_4S_8 and GaV_4S_8. *Chem. Mater.* **18**, 2174–2180 (2006).
18. Dorolti, E. et al. Half-metallic ferromagnetism and large negative magnetoresistance in the new lacunar spinel $GaTi_3VS_8$. *J. Am. Chem. Soc.* **132**, 5704–5710 (2010).
19. Singh, K. et al. Orbital-ordering-driven multiferroicity and magnetoelectric coupling in GeV_4S_8. *Phys. Rev. Lett.* **113**, 137602 (2014).
20. Xu, K. & Xiang, H. J. Unusual ferroelectricity induced by the Jahn-Teller effect: a case study on lacunar spinel compounds. *Phys. Rev. B* **92**, 121112 (2015).
21. Sieberer, M., Turnovszky, S., Redinger, J. & Mohn, P. Importance of cluster distortions in the tetrahedral cluster compounds GaM_4X_8 (M = Mo, V, Nb, Ta; X = S, Se): Ab initio investigations. *Phys. Rev. B* **76**, 214106 (2007).
22. Pocha, R., Johrendt, D., Ni, B. & Abd-Elmeguid, M. M. Crystal structures, electronic properties, and pressure-induced superconductivity of the tetrahedral cluster compounds $GaNb_4S_8$, $GaNb_4Se_8$, and $GaTa_4Se_8$. *J. Am. Chem. Soc.* **127**, 8732–8740 (2005). PMID: 15954779.
23. Guiot, V. et al. Avalanche breakdown in $GaTa_4Se_{8-x}Te_x$ narrow-gap Mott insulators. *Nat. Commun.* **4**, 1722 (2013).
24. Guiot, V., Janod, E., Corraze, B. & Cario, L. Control of the electronic properties and resistive switching in the new series of Mott insulators $GaTa_4Se_{8-y}Te_y (0 \le y \le 6.5)$. *Chem. Mater.* **23**, 2611–2618 (2011).
25. Vaju, C. et al. Electric-pulse-driven electronic phase separation, insulator-metal transition, and possible superconductivity in a Mott insulator. *Adv. Mater.* **20**, 2760–2765 (2008).
26. Dubost, V. et al. Resistive switching at the nanoscale in the Mott insulator compound $GaTa_4Se_8$. *Nano Lett.* **13**, 3648–3653 (2013).
27. Cario, L., Vaju, C., Corraze, B., Guiot, V. & Janod, E. Electric-field-induced resistive switching in a family of Mott insulators: towards a new Class of RRAM Memories. *Adv. Mater.* **22**, 5193–5197 (2010).
28. Kim, H.-S., Im, J., Han, M. J. & Jin, H. Spin-orbital entangled molecular j_{eff} states in lacunar spinel compounds. *Nat. commun.* **5**, 3988 (2014).
29. Jeong, M. Y. et al. Direct experimental observation of the molecular Jeff = 3/2 ground state in the lacunar spinel $GaTa_4Se_8$. *Nat. Commun.* **8**, 782 (2017).
30. Abd-Elmeguid, M. M. et al. Transition from Mott insulator to superconductor in $GaNb_4$ Se_8 and $GaTa_4$ Se_8 under high pressure. *Phys. Rev. Lett.* **93**, 126403 (2004).
31. Ta Phuoc, V. et al. Optical conductivity measurements of $GaTa_4Se_8$ under high pressure: evidence of a bandwidth-controlled insulator-to-metal Mott transition. *Phys. Rev. Lett.* **110**, 037401 (2013).
32. Camjayi, A. et al. First-order insulator-to-metal Mott transition in the paramagnetic 3D system $GaTa_4Se_8$. *Phys. Rev. Lett.* **113**, 086404 (2014).
33. Jakob, S. et al. Structural and magnetic transitions in the Mott insulator $GaNb_4S_8$. *J. Mater. Chem.* **17**, 3833–3838 (2007).
34. Yaich, H. et al. Nouveaux chalcogénures et chalcohalogénures à clusters tétraédriques Nb_4 ou Ta_4. *J. Less Common Met.* **102**, 9–22 (1984).
35. Kawamoto, S. et al. Frustrated magnetism in a Mott insulator based on a transition metal chalcogenide. *J. Phys.: Conference Series* **683**, 012025 (2016).
36. Waki, T. et al. Spin-singlet state formation in the cluster Mott insulator $GaNb_4S_8$ studied by μ SR and NMR spectroscopy. *Phys. Rev. B* **81**, 020401 (2010).
37. Menke, H., Timm, C. & Brydon, P. M. R. Bogoliubov Fermi surfaces stabilized by spin-orbit coupling. *Phys. Rev. B* **100**, 224505 (2019).
38. Savary, L., Ruhman, J., Venderbos, J. W. F., Fu, L. & Lee, P. A. Superconductivity in three-dimensional spin-orbit coupled semimetals. *Phys. Rev. B* **96**, 214514 (2017).
39. Boettcher, I. & Herbut, I. F. Unconventional superconductivity in Luttinger semimetals: theory of complex tensor order and the emergence of the uniaxial nematic state. *Phys. Rev. Lett.* **120**, 057002 (2018).
40. Agterberg, D. F., Brydon, P. M. R. & Timm, C. Bogoliubov Fermi surfaces in superconductors with broken time-reversal symmetry. *Phys. Rev. Lett.* **118**, 127001 (2017).
41. Roy, B., Ghorashi, S. A. A., Foster, M. S. & Nevidomskyy, A. H. Topological superconductivity of spin-3/2 carriers in a three-dimensional doped Luttinger semimetal. *Phys. Rev. B* **99**, 054505 (2019).
42. Venderbos, J. W. F., Savary, L., Ruhman, J., Lee, P. A. & Fu, L. Pairing states of spin $\frac{3}{2}$ fermions: symmetry-enforced topological gap functions. *Phys. Rev. X* **8**, 011029 (2018).
43. Brydon, P. M. R., Wang, L., Weinert, M. & Agterberg, D. F. Pairing of $j = 3/2$ fermions in half-heusler superconductors. *Phys. Rev. Lett.* **116**, 177001 (2016).

44. Chen, G. & Balents, L. Spin-orbit coupling in d^2 ordered double perovskites. *Phys. Rev. B* **84**, 094420 (2011).
45. Cheung, A. K. C. & Agterberg, D. F. Superconductivity in the presence of spin-orbit interactions stabilized by Hund coupling. *Phys. Rev. B* **99**, 024516 (2019).
46. Bravyi, S., DiVincenzo, D. P. & Loss, D. Schrieffer-Wolff transformation for quantum many-body systems. *Ann. Phy.* **326**, 2793–2826 (2011).
47. Chiu, C.-K., Teo, J. C. Y., Schnyder, A. P. & Ryu, S. Classification of topological quantum matter with symmetries. *Rev. Mod. Phys.* **88**, 035005 (2016).
48. Wang, D. et al. Evidence for Majorana bound states in an iron-based superconductor. *Science* **362**, 333–335 (2018).
49. Chen, A., Pikulin, D. I. & Franz, M. Josephson current signatures of Majorana flat bands on the surface of time-reversal-invariant Weyl and Dirac semimetals. *Phys. Rev. B* **95**, 174505 (2017).
50. Chen, A. & Franz, M. Superconducting proximity effect and Majorana flat bands at the surface of a Weyl semimetal. *Phys. Rev. B* **93**, 201105 (2016).
51. Yang, Z., Qin, S., Zhang, Q., Fang, C. & Hu, J. $\pi/2$-Josephson junction as a topological superconductor. *Phys. Rev. B* **98**, 104515 (2018).
52. Wollman, D. A., Van Harlingen, D. J., Lee, W. C., Ginsberg, D. M. & Leggett, A. J. Experimental determination of the superconducting pairing state in YBCO from the phase coherence of YBCO-Pb dc SQUIDs. *Phys. Rev. Lett.* **71**, 2134–2137 (1993).
53. Wollman, D. A., Van Harlingen, D. J., Giapintzakis, J. & Ginsberg, D. M. Evidence for $d_{x^2-y^2}$ pairing from the magnetic Field modulation of $YBa_2Cu_3O_7$-Pb Josephson junctions. *Phys. Rev. Lett.* **74**, 797–800 (1995).
54. Van Harlingen, D. J. Phase-sensitive tests of the symmetry of the pairing state in the high-temperature superconductors—evidence for $d_{x^2-y^2}$ symmetry. *Rev. Mod. Phys.* **67**, 515–535 (1995).
55. Park, M. J., Yang, J., Kim, Y. & Gilbert, M. J. Fulde-Ferrell states in inverse proximity-coupled magnetically doped topological heterostructures. *Phys. Rev. B* **96**, 064518 (2017).
56. Chen, A. Q. et al. Finite momentum Cooper pairing in three-dimensional topological insulator Josephson junctions. *Nat. Commun.* **9**, 3478 (2018).
57. Ozaki, T. Variationally optimized atomic orbitals for large-scale electronic structures. *Phys. Rev. B* **67**, 155108 (2003).
58. Ceperley, D. M. & Alder, B. Ground state of the electron gas by a stochastic method. *Phys. Rev. Lett.* **45**, 566 (1980).
59. Perdew, J. P. & Zunger, A. Self-interaction correction to density-functional approximations for many-electron systems. *Phys. Rev. B* **23**, 5048 (1981).
60. MacDonald, A. H. & Vosko, S. H. A relativistic density functional formalism. *J. Phys. C: Solid State Phys.* **12**, 2977–2990 (1979).
61. Marzari, N. & Vanderbilt, D. Maximally localized generalized Wannier functions for composite energy bands. *Phys. Rev. B* **56**, 12847–12865 (1997).
62. Souza, I., Marzari, N. & Vanderbilt, D. Maximally localized Wannier functions for entangled energy bands. *Phys. Rev. B* **65**, 035109 (2001).
63. Aryasetiawan, F. et al. Frequency-dependent local interactions and low-energy effective models from electronic structure calculations. *Phys. Rev. B* **70**, 195104 (2004).
64. Miyake, T. & Aryasetiawan, F. Screened Coulomb interaction in the maximally localized Wannier basis. *Phys. Rev. B* **77**, 085122 (2008).
65. Şaşioğlu, E., Friedrich, C. & Blügel, S. Effective Coulomb interaction in transition metals from constrained random-phase approximation. *Phys. Rev. B* **83**, 121101 (2011).
66. Kotani, T. First-principles electronic structure calculation code, ecalj package (https://github.com/tkotani/ecalj).

ACKNOWLEDGEMENTS

M.Y.J. and M.J.H. are grateful to Jungho Kim, Seo Hyoung Chang, and Seung Woo Jang for fruitful discussion. M.Y.J. and M.J.H. were supported by Basic Science Research Program (2018R1A2B2005204) and Creative Materials Discovery Program (2018M3D1A1058754) through the National Research Foundation of Korea (NRF) funded by the Ministry of Science and ICT. M.J.P., G.B.S., and S.B.L. are supported by the KAIST startup, BK21 and National Research Foundation Grant (NRF-2017R1A2B4008097).

AUTHOR CONTRIBUTIONS

S.B.L. and M.J.H. conceived and supervised the research. M.J.P., G.B.S., and M.Y.J performed the calculations in this work. A.M. provided preliminary results regarding the Fierz transformation, and contributed to the discussion of the quintet pairing superconductivity. All authors contributed to writing the paper.

COMPETING INTERESTS

The authors declare no competing interests.

ADDITIONAL INFORMATION

Supplementary information is available for this paper at https://doi.org/10.1038/s41535-020-0246-0.

Correspondence and requests for materials should be addressed to M.J.H. or S.L.

Reprints and permission information is available at http://www.nature.com/reprints

Publisher's note Springer Nature remains neutral with regard to jurisdictional claims in published maps and institutional affiliations.